Hybrid CARS spectroscopy based on a high-repetition-rate all-PM-fiber laser source

Cao, Tao; Yan, Jikun; Chen, Yu; Huang, Le; Guo, Ziyue; Liu, Shaozhen; Hu, Kailin; Ridsdale, Andrew; Sokolov, Alexei V.; Peng, Jiahui

Publisher's version / Version de l'éditeur:
https://doi.org/10.1063/5.0020728
Applied Physics Letters, 117, 8, pp. 1-5, 2020-08-25

Applied Physics Letters

Hybrid CARS spectroscopy based on a high-repetition-rate all-PM-fiber laser source

Cite as: Appl. Phys. Lett. **117**, 081103 (2020); https://doi.org/10.1063/5.0020728
Submitted: 03 July 2020 . Accepted: 07 August 2020 . Published Online: 25 August 2020

Tao Cao, Jikun Yan, Yu Chen, Le Huang, Ziyue Guo, Shaozhen Liu, Kailin Hu, Andrew Ridsdale, Alexei V. Sokolov, and Jiahui Peng

Applied Physics Letters ARTICLE scitation.org/journal/apl

Hybrid CARS spectroscopy based on a high-repetition-rate all-PM-fiber laser source

Cite as: Appl. Phys. Lett. **117**, 081103 (2020); doi: 10.1063/5.0020728
Submitted: 3 July 2020 · Accepted: 7 August 2020 ·
Published Online: 25 August 2020

Tao Cao,[1,a)] Jikun Yan,[1] Yu Chen,[1] Le Huang,[1] Ziyue Guo,[1] Shaozhen Liu,[1] Kailin Hu,[1] Andrew Ridsdale,[2,b)] Alexei V. Sokolov,[3,c)] and Jiahui Peng[1,d)]

AFFILIATIONS

[1]School of Optical and Electronic Information, Huazhong University of Science and Technology, Wuhan 430074, China
[2]Security and Disruptive Technologies Research Center, National Research Council of Canada, Ottawa, Ontario K1A 0R6, Canada
[3]Department of Physics and Astronomy and Institute for Quantum Science and Engineering, Texas A&M University, College Station, Texas 77843-4242, USA

[a)]Author to whom correspondence should be addressed: caotao@hust.edu.cn
[b)]Electronic mail: Andrew.Ridsdale@nrc-cnrc.gc.ca
[c)]Electronic mail: sokol@physics.tamu.edu
[d)]Electronic mail: jpeng@hust.edu.cn

ABSTRACT

We demonstrate a robust, simple, and compact all polarization-maintaining (PM) fiber laser source with a repetition rate of 79 MHz for broadband coherent anti-Stokes Raman scattering (CARS) spectroscopy based on impulsive excitation and narrowband probing. The careful dispersion management during the generation of pump pulses ensures efficient impulsive excitation, which is verified to cover an ultrabroad bandwidth exceeding 4000 cm^{-1}. The employment of PM fibers enables the laser source to withstand external disturbances. This turn-key configuration can potentially simplify the implementation of many applications of CARS, such as spectroscopic histopathology, weaponized endospore detection, and precise thermometry of gases.

Coherent anti-Stokes Raman scattering (CARS) is a noninvasive and label-free spectroscopic technique.[1] The strong signal created has enabled video-rate chemically specific microscope imaging of biological samples by capturing a single Raman peak.[2] To further differentiate components in complex heterogeneous systems such as cells, tissues, and minerals, several methods aiming at rapidly acquiring multiple Raman peaks have been developed, including spectral focusing,[3] multiplex,[4] single-beam,[5] Fourier-transform,[6] and hybrid[7–9] CARS techniques. These broadband CARS techniques generally involve ultrafast Ti:sapphire lasers and parametric frequency conversion systems. In order to circumvent such technologically challenging demands, fiber-laser technologies are exploited. More specifically, ultrafast fiber lasers are employed for synchronized dual-pulse generation. Fiber-based supercontinuum (SC) generation aids in frequency extension.[10–12]

Here, we present an all polarization-maintaining (PM) fiber laser source for hybrid CARS. This CARS technique can acquire information comparable to that of spontaneous Raman spectroscopy at a much higher speed. This method has been applied to various fields, such as spectroscopic histopathology,[13] weaponized endospore detection,[8] and precise thermometry of gases.[14–16] This technique was first implemented with a three-beam scheme and later simplified to a two-beam scheme.[17,18] In the two-beam scheme, a well-compressed broadband laser pulse provides pump and Stokes photons simultaneously, and a synchronized narrowband laser pulse provides the probe. The generated CARS spectra are captured by frequency-resolved multi-channel detection. The well-compressed broadband pulse enables efficient impulsive excitation. This makes efficient excitation across the whole fingerprint region possible, where abundant CARS peaks appear with relatively low intensity.

However, the non-resonant background (NRB) induced by instantaneous electronic-response four-wave mixing often degrades the molecular specificity of CARS spectroscopy. This often limits the application of CARS spectroscopy outside of the gas phase. In hybrid CARS, introducing a delay between the probe pulse and the pump pulse can eliminate the NRB, because CARS signals usually decay slower than the NRB as the inter-pulse delay increases.[19] Meanwhile,

the vibrational dynamics of molecules can be captured by recording Raman peak intensities as a function of the delay.

Although various fiber-based laser sources have been developed for CARS spectroscopy and microscopy,[20] only a few of them can be used for hybrid CARS.[10] Among those laser sources for hybrid CARS, the majority still contains free-space optics. The main obstacle on the path to an all-fiber format is large and often complex chirp in the broadband pump pulse. This degrades the impulsive excitation in the CARS process. In order to better control the pump chirp, parameters of the input pulse[21] and the length of the nonlinear fiber[22] must be adjusted for optimal SC generation.

We adopted several strategies in our laser source accordingly. First, self-similar amplification is exploited for simultaneously scaling up the energy and bandwidth of seed pulses,[23] enabling high peak intensity for SC generation after pulse compression. Second, optimal pre-chirp for SC generation is achieved through employing a dispersion compensation fiber (DCF) with a proper length. This method works because self-similar amplification only introduces a positive linear chirp. Finally, a zero-dispersion highly nonlinear fiber (HNLF) cut to an optimal length minimizes the chirp introduced during SC generation and, thus, suppresses pulse breaking.[24]

The schematic of our hybrid CARS system is shown in Fig. 1. The seed is a home-made self-starting erbium-doped mode-locked oscillator. This oscillator delivers a 79 MHz pulse train with an average power of 1.78 mW and a bandwidth of 18 nm. Its repetition rate can be easily optimized to 200 MHz by shortening the length of its linear arm. Pedestal suppression by the nonlinear loop mirror[25] assures an output spectrum without Kelly bands,[26] as shown in Fig. 2(a).

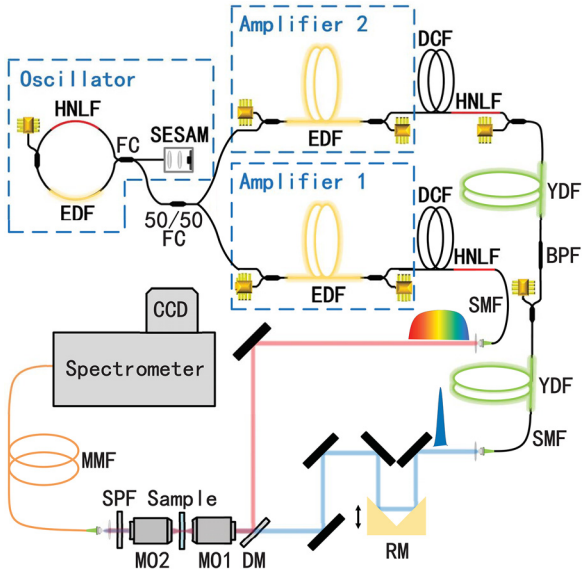

FIG. 1. Schematic of the hybrid CARS system: SESAM, semiconductor saturable absorption mirror; FC, fiber coupler; HNLF, highly nonlinear fiber; EDF, Er-doped fiber; DCF, dispersion compensation fiber; YDF, Yb-doped fiber; BPF, 3-nm bandpass filter centered at 1064 nm; RM, gold-coated roof mirror mounted on a translation stage; DM, dichroic mirror; MO, microscope objective. SPF, shortpass filter cut off at 1000 nm; SMF, single-mode fiber; MMF, multimode fiber. All the fibers are polarization-maintaining.

The oscillator seeds two parallel single-stage Er-doped fiber amplifiers with equal powers. Each amplifier scales the laser power up to 180 mW. Broadened spectra with bandwidths of 60 nm are obtained, as shown in Fig. 2(b). Such a spectrum enables a pulse duration below 100 fs after compression. This allows the generation of octave-spanning SC in a short HNLF with a moderate chirp.[24]

Amplifier 1 is deployed in the broadband branch, as shown in Fig. 1. This branch generates broadband pump pulses with an average power of 38 mW for impulsive excitation in the CARS process. A DCF compresses the linearly chirped pulse generated by amplifier 1, which is then delivered to a HNLF with zero group delay dispersion (GDD) at 1550 nm for SC generation. The length of the DCF is optimized to obtain the broadest SC. The HNLF is cut to a moderately short length (17.5 cm) without reducing the SC bandwidth. As shown in Fig. 2(c), the spectrum of the generated SC spans from 1100 nm to over 1700 nm. Spectral components over 1700 nm are beyond the measurement range of our optical spectral analyzer. However, the NRB generated in the CARS process indicates a pump bandwidth exceeding 4000 cm^{-1}. Ultrashort laser pulses with such a bandwidth can excite almost all molecular vibrations accessible to Raman spectroscopy.

For a convenient output format, a standard SMF pigtail is spliced to the HNLF. The length of the DCF is further adjusted to provide moderate pre-chirp in order to compensate the dispersion of optics outside the laser source. The optimal length is achieved when a BBO powder smear at the focus generates the strongest second harmonic.

Amplifier 2 is deployed in the narrowband branch, as shown in Fig. 1. This branch generates narrowband probe pulses with an average power of 180 mW. The lengths of the SMF and the HNLF are optimized to transfer sufficient power to 1064 nm, producing SC as shown in Fig. 2(c). The SC seeds a YDF, filtered by a 3-nm bandpass fiber filter and successively amplified by another YDF. An SMF pigtail delivers the generated narrowband pulses to the output port. The output spectrum is shown in Fig. 2(d). The probe pulse has a linewidth of

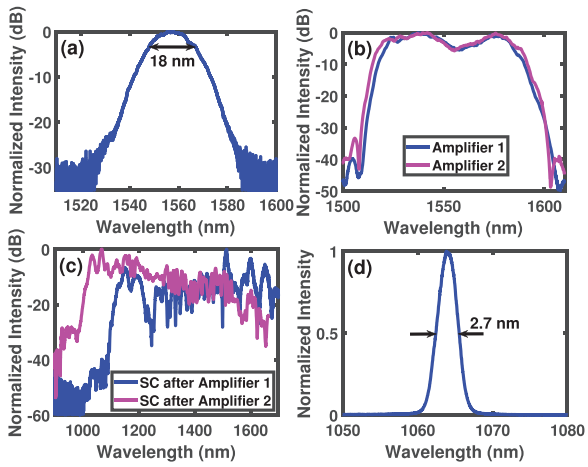

FIG. 2. (a) Output spectrum of the oscillator. The FWHM bandwidth is 18 nm. (b) Output spectra of amplifiers 1 and 2. (c) Spectra of supercontinua generated by the HNLF after amplifiers 1 and 2. Spectra above 1700 nm are beyond the measurement range of our spectrometer. (d) Spectrum of the probe. The FWHM linewidth is 2.7 nm.

2.7 nm and a center wavelength of 1064 nm, corresponding to a linewidth of 24 cm^{-1}. A narrower linewidth can be further attained by replacing the filter with a narrower-bandwidth one or a fiber Bragg grating so that higher-resolution CARS spectra can be obtained.

The laser source is fully composed of PM fibers. Consequently, pump and probe beams generated by the laser source are locked to the same linear polarization direction, staying robust against external disturbances and remaining in a constant state after repeated starts and stops of the system. Therefore, optimal polarization matching for CARS signal generation is guaranteed without the need for additional adjustments of free-space polarization optics.

The dispersion management in the laser source makes additional free-space dispersion compensation unnecessary in the pump line. A roof mirror mounted on a transition stage is employed in the probe-delay tuning. A dichroic mirror combines pump and probe beams, which are then delivered to an achromatic objective lens (NA = 0.4) for focusing. The laser beam transmitted through the sample is then collimated by another objective lens (NA = 0.1), filtered by a shortpass filter cut off at 1000 nm, and coupled to a spectrograph (Andor SR-303i-B) by a multimode fiber patch code. A CCD camera (Andor DU416A-LDC-DD) is employed to record the CARS spectra.

To test the performance of this system, pure benzene is employed for CARS signal generation. The pump and probe powers measured after the focusing objective (labeled as MO1 in Fig. 1) are 18 mW and 38 mW, respectively. CARS spectra varying with the probe delay are shown in Fig. 3(a). The zero delay time is defined as when the total photon count reaches maximum. The positive delay time signifies that the probe pulse lags behind the pump pulse. The three labeled peaks surviving well beyond 2 ps after zero delay time are produced by molecular vibrations. The broadband background ranging approximately from 600 cm^{-1} to 4300 cm^{-1} is the NRB, which decays at the same rate as that of the probe's tailing edge. Since impulsive excitation provides frequency detuning starting from 0 cm^{-1}, the high frequency cutoff of the NRB indicates that the excitation bandwidth exceeds 4000 cm^{-1}. This confirms an ultrabroad pump bandwidth as mentioned previously.

With impulsive excitation, a very strong NRB is generated when the probe pulse overlaps with the pump pulse, as shown in Fig. 3(b). The NRB overwhelms some weak Raman peaks such as those located at 606 cm^{-1} and 849 cm^{-1}. However, it can be removed by increasing the probe delay. When the delay reaches 3 ps, a clean spectrum resembling that produced by spontaneous Raman spectroscopy is obtained, as shown in Fig. 3(c). In this figure, Raman peaks of benzene at 606 cm^{-1}, 849 cm^{-1}, 992 cm^{-1}, and 3062 cm^{-1} are readily discernible.

When the pump pulse is not well compressed, two-color excitation contributes more to CARS signals than impulsive excitation.[17] However, two-color excitation prevents the use of a delayed probe pulse to reject the NRB and keep the resonant contribution, because it employs a single pulse for pumping and probing. Therefore, the spectrum shown in Fig. 3(c) verifies the existence of impulsive excitation. Furthermore, in order to characterize the proportions of signals generated by impulsive excitation, intensities of the 606 cm^{-1} peak and the 3062 cm^{-1} peak at zero probe delay are plotted as a function of the probe power, as shown in Figs. 4(a) and 4(b). Linear fitting in log-log coordinates gives slopes of 1.17 and 1.13 at 606 cm^{-1} and 3062 cm^{-1}, respectively. Such an approximately linear dependence of the CARS signal on the probe power also confirms that impulsive excitation dominates over two-color excitation even at zero probe delay.[17]

Because efficient impulsive excitation can only be achieved by well compressed pump pulses, it is important to monitor the chirp of pump pulses. This information has been hidden in the time-resolved CARS intensity $I_{aS}(\tau, \omega)$. Since the bandwidth of probe pulses is much narrower than that of pump pulses, the time-resolved CARS amplitude induced by impulsive excitation can be written as

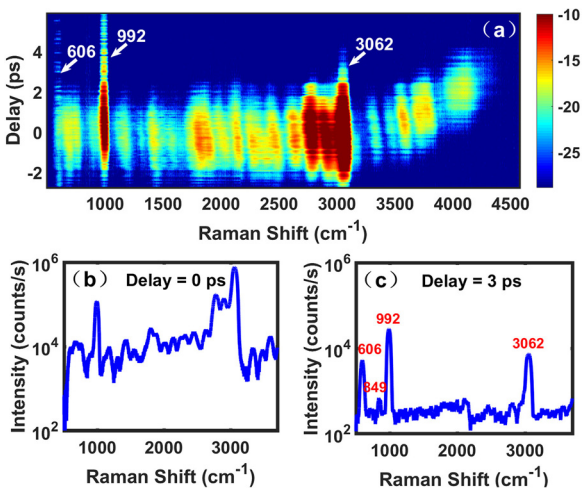

FIG. 3. (a) Time-resolved CARS spectrum of benzene. (b) and (c) CARS spectra of benzene at zero and 3 ps probe delay. Frequency components below 600 cm^{-1} are cut out by the short pass filter. The exposure time of the CCD is 71.62 ms.

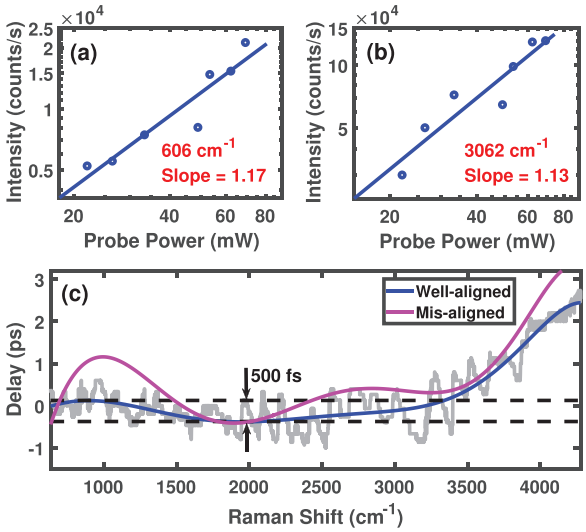

FIG. 4. Intensities of (a) the 606 cm^{-1} peak and (b) the 3062 cm^{-1} peak at zero probe delay plotted as a function of the probe power at the sample. Slopes are obtained by linearly fitting log–log plots of the peak intensities. (c) Frequency-dependent delay of the self-correlation of the pump field plotted as a function of the Raman shift. The gray curve is measured experimentally, and the blue curve is its seventh order polynomial fitting with the system well aligned. The magenta curve is obtained in the same way as the blue one with the system slightly misaligned.

$$\sqrt{I_{aS}(\tau,\omega)} \approx |S(\omega)| \times \left| \int_{-\infty}^{+\infty} \chi^{(3)}(\Omega) e^{i[T(\omega)(\Omega-\omega)+\phi(\omega)]} \times E_{pr}(\omega-\Omega) e^{i(\omega-\Omega)\tau} d\Omega \right| = |S(\omega)| \times \left| \mathscr{F}\left[\chi^{(3)}(\Omega) E_{pr}(\omega-\Omega) e^{iT(\omega)\Omega}\right] \right|, \quad (1)$$

where τ is the probe delay, ω is the frequency shift relative to the central frequency of the probe pulse (Raman shift), $S(\omega)$ is the self-correlation of the pump field, $\chi^{(3)}(\Omega)$ is the third-order nonlinear susceptibility, $E_{pr}(\omega-\Omega)$ is the probe field, $\mathscr{F}$ is the Fourier transform operator, and $T(\omega)(\Omega-\omega)+\phi(\omega)$ is a linear fitting of the spectral phase of $S(\Omega)$ in the vicinity of ω. Since the derivative of the spectral phase of a pulse is equivalent to its frequency-dependent delay, $T(\omega)$ gives an indication of the chirp of the pump field self-correlation.

In Fourier transform, a phase shift in frequency domain corresponds to a time shift in time domain. Hence, Eq. (1) implies that the frequency-dependent delay of the pump field self-correlation corresponds to the time shift of the CARS signal intensity along the delay axis. Such a time shift can be quantified by the time deviation of the maximum intensity point from zero delay. Therefore, the chirp of the pump field self-correlation can be visualized by plotting the time shift as a function of the Raman shift ω, as shown in Fig. 4(c). The blue curve represents a 7th order polynomial fitting of the experimental data (gray line). The magenta curve is the frequency-dependent delay curve measured when the CARS system was slightly misaligned. The deviation of the magenta curve from the blue one reflects the additive chirp introduced by the misalignment, indicating this curve's sensitivity to the chirp change of the pump.

Such *in situ* measured frequency-dependent delay curves reflect the chirp features of pump fields and provide feedback for optimizing the dispersion management in the laser source. The frequency-dependent delay below 3340 cm^{-1} is restricted within a time range of 500 fs, as shown in Fig. 4(c). This result suggests the possibility to further improve the dispersion management in the laser source. Further improvements may include optimizing the gain value of the EDF employed for self-similar amplification, whereby pulses with a higher energy and broader bandwidth can be obtained after the amplification.[27] Under this circumstance, higher peak intensity can be achieved after pulse compression, which results in SC generation in a shorter HNLF and, thus, less introduced chirp.

In conclusion, we demonstrate a robust, simple, and compact all-PM-fiber laser source for hybrid CARS. In order to achieve efficient impulsive excitation in the CARS process, we implement careful dispersion management in the laser source to obtain optimally compressed pump pulses for CARS excitation. Additionally, the laser source is fully composed of PM fibers, making it able to withstand external disturbances. The hybrid CARS system is applied to benzene, verifying that vibrational coherence established by impulsive excitation covers a frequency range exceeding 4000 cm^{-1}. This system can be further integrated by using fibers to delay the probe pulses and an endlessly single-mode large-mode-area photonic crystal fiber to transmit the pump and probe pulses. This turn-key configuration can potentially popularize broadband CARS spectroscopy in more applications outside of a laboratory environment.

We wish to acknowledge financial support from the National Key R&D Plan of China (No. 2016YFB1102404), the Technological Innovation Major Project of Hubei Province (No. 2016AAA004), the Open Fund of the State Key Laboratory of High Field Laser Physics (Shanghai Institute of Optics and Fine Mechanics), and the Robert A. Welch Foundation (Award No. A-1547).

DATA AVAILABILITY

The data that support the findings of this study are available from the corresponding author upon reasonable request.

REFERENCES

[1] D. W. Shipp, F. Sinjab, and I. Notingher, "Raman spectroscopy: Techniques and applications in the life sciences," Adv. Opt. Photonics **9**, 315–428 (2017).
[2] A. Zumbusch, G. R. Holtom, and X. S. Xie, "Three-dimensional vibrational imaging by coherent anti-stokes Raman scattering," Phys. Rev. Lett. **82**, 4142 (1999).
[3] T. Hellerer, A. M. Enejder, and A. Zumbusch, "Spectral focusing: High spectral resolution spectroscopy with broad-bandwidth laser pulses," Appl. Phys. Lett. **85**, 25–27 (2004).
[4] M. Müller and J. M. Schins, "Imaging the thermodynamic state of lipid membranes with multiplex CARS microscopy," J. Phys. Chem. B **106**, 3715–3723 (2002).
[5] N. Dudovich, D. Oron, and Y. Silberberg, "Single-pulse coherently controlled nonlinear Raman spectroscopy and microscopy," Nature **418**, 512 (2002).
[6] M. Cui, M. Joffre, J. Skodack, and J. P. Ogilvie, "Interferometric fourier transform coherent anti-stokes Raman scattering," Opt. Express **14**, 8448–8458 (2006).
[7] B. D. Prince, A. Chakraborty, B. M. Prince, and H. U. Stauffer, "Development of simultaneous frequency- and time-resolved coherent anti-stokes Raman scattering for ultrafast detection of molecular Raman spectra," J. Chem. Phys. **125**, 044502 (2006).
[8] D. Pestov, R. K. Murawski, G. O. Ariunbold, X. Wang, M. Zhi, A. V. Sokolov, V. A. Sautenkov, Y. V. Rostovtsev, A. Dogariu, and Y. Huang, "Optimizing the laser-pulse configuration for coherent Raman spectroscopy," Science **316**, 265–268 (2007).
[9] V. Kumar, R. Osellame, R. Ramponi, G. Cerullo, and M. Marangoni, "Background-free broadband CARS spectroscopy from a 1-MHz ytterbium laser," Opt. Express **19**, 15143–15148 (2011).
[10] R. Selm, M. Winterhalder, A. Zumbusch, G. Krauss, T. Hanke, A. Sell, and A. Leitenstorfer, "Ultrabroadband background-free coherent anti-stokes Raman scattering microscopy based on a compact Er: Fiber laser system," Opt. Lett. **35**, 3282–3284 (2010).
[11] T. Gottschall, M. Baumgartl, A. Sagnier, J. Rothhardt, C. Jauregui, J. Limpert, and A. Tünnermann, "Fiber-based source for multiplex-CARS microscopy based on degenerate four-wave mixing," Opt. Express **20**, 12004–12013 (2012).
[12] Y. Li, X. Xiao, J. Guo, K. Zhao, S. Yao, L. Gui, and C. Yang, "Multimodal coherent anti-stokes Raman scattering microscopy with a supercontinuum all-fiber laser," IEEE Photonics J. **11**, 1–8 (2019).
[13] J. Camp, H. Charles, Y. J. Lee, J. M. Heddleston, C. M. Hartshorn, A. R. H. Walker, J. N. Rich, J. D. Lathia, and M. T. Cicerone, "High-speed coherent Raman fingerprint imaging of biological tissues," Nat. Photonics **8**, 627–634 (2014).
[14] R. Santagata, M. Scherman, M. Toubeix, M. Nafa, B. Tretout, and A. Bresson, "Ultrafast background-free ro-vibrational fs/ps-CARS thermometry using an Yb: YAG crystal-fiber amplified probe," Opt. Express **27**, 32924–32937 (2019).
[15] J. D. Miller, M. N. Slipchenko, T. R. Meyer, H. U. Stauffer, and J. R. Gord, "Hybrid femtosecond/picosecond coherent anti-stokes Raman scattering for high-speed gas-phase thermometry," Opt. Lett. **35**, 2430–2432 (2010).
[16] A. Bohlin and C. J. Kliewer, "Direct coherent Raman temperature imaging and wideband chemical detection in a hydrocarbon flat flame," J. Phys. Chem. Lett. **6**, 643–649 (2015).
[17] Y. J. Lee, Y. Liu, and M. T. Cicerone, "Characterization of three-color CARS in a two-pulse broadband CARS spectrum," Opt. Lett. **32**, 3370–3372 (2007).
[18] K. Shi, P. Li, and Z. Liu, "Broadband coherent anti-stokes Raman scattering spectroscopy in supercontinuum optical trap," Appl. Phys. Lett. **90**, 141116 (2007).

[19]A. Laubereau and W. Kaiser, "Vibrational dynamics of liquids and solids investigated by picosecond light pulses," Rev. Mod. Phys. **50**, 607–665 (1978).
[20]T. Gottschall, T. Meyer, M. Baumgartl, C. Jauregui, M. Schmitt, J. Popp, J. Limpert, and A. Tunnermann, "Fiber-based light sources for biomedical applications of coherent anti-stokes Raman scattering microscopy," Laser Photonics Rev. **9**, 435–451 (2015).
[21]Y. J. Lee, S. H. Parekh, Y. H. Kim, and M. T. Cicerone, "Optimized continuum from a photonic crystal fiber for broadband time-resolved coherent anti-stokes Raman scattering," Opt. Express **18**, 4371–4379 (2010).
[22]H. Kano and H. O. Hamaguchi, "Dispersion-compensated supercontinuum generation for ultrabroadband multiplex coherent anti-stokes Raman scattering spectroscopy," J. Raman Spectrosc. **37**, 411–415 (2006).
[23]M. E. Fermann, V. I. Kruglov, B. C. Thomsen, J. M. Dudley, and J. D. Harvey, "Self-similar propagation and amplification of parabolic pulses in optical fibers," Phys. Rev. Lett. **84**, 6010–6013 (2000).
[24]J. M. Dudley, G. Genty, and S. Coen, "Supercontinuum generation in photonic crystal fiber," Rev. Mod. Phys. **78**, 1135–1184 (2006).
[25]K. Smith, N. J. Doran, and P. G. J. Wigley, "Pulse shaping, compression, and pedestal suppression employing a nonlinear-optical loop mirror," Opt. Lett. **15**, 1294–1296 (1990).
[26]S. M. J. Kelly, "Characteristic sideband instability of periodically amplified average soliton," Electron. Lett. **28**, 806–807 (1992).
[27]G. Chang, A. Galvanauskas, H. G. Winful, and T. B. Norris, "Dependence of parabolic pulse amplification on stimulated Raman scattering and gain bandwidth," Opt. Lett. **29**, 2647–2649 (2004).